# Thermodynamic Properties of $Me_2Ni_{17}$ (Me = Sm, Dy, and Yb) Intermetallics by Solid Electrolyte Cells under Effusion Conditions

**F. Di Pascasio and D. Gozzi***

*Dipartimento di Chimica, Università di Roma La Sapienza, P.le A. Moro 5, 00185 Roma, Italy*

**N. Parodi and G. Borzone**

*Dipartimento di Chimica e Chimica Industriale, Università di Genova, Via Dodecaneso, 31 16146 Genova, Italy*

*Received: November 20, 2001; In Final Form: February 12, 2002*

The purpose of this work is to contribute to rare earth/3d metal thermodynamics of systems not experimentally determined prior to this research. The thermodynamics of the Ni-rich phase, $Me_2Ni_{17}$, in the binary systems Me-Ni, with Me = Sm, Dy, and Yb, has been studied in the temperature range from 900 to 1200 K by a new experimental setup based on solid-state galvanic cells with $CaF_2$ single crystal as the solid electrolyte. This is particularly useful when the vapor pressure of one of the components of the electrochemical cell is high at the working temperature. The electromotive force method has been adopted to obtain the thermodynamic properties of the intermetallics under investigation. Their $\Delta_f H^{\theta}_T$ values have been found to be $-14.6 \pm 0.5$, $-18.5 \pm 0.1$, and $-17.0 \pm 0.1$ kJ/mol atoms, respectively, for $Sm_2Ni_{17}$ and $Dy_2Ni_{17}$ at $T = 298$ K and $Yb_2Ni_{17}$ at $T = 990$ K. These values agree well with the calculated values obtained through the Miedema model. Values of the activity of Me in the Ni solid solution in thermodynamic equilibrium with the respective $Me_2Ni_{17}$ phase were calculated at 1000 K to be $6.8 \times 10^{-10}$, $4.8 \times 10^{-10}$, and $1.5 \times 10^{-10}$, respectively, for Sm, Dy, and Yb. The activity against the Me atomic volume was also investigated together with the physical meaning of the partial excess free energy change of the Ni solid solution.

## 1. Introduction

There are several theoretical and technological reasons to study the alloys and intermetallic compounds between 3d transition metals and rare earth elements. The theoretical interest is mostly confined to the solid-state physics particularly as it concerns the magnetic and superconductivity properties. Practical applications are even more relevant, especially those related to the storage of hydrogen, rechargeable batteries, and permanent magnets. From the point of view of their physicochemical properties, particularly phase diagrams and the related thermodynamics, a much work has been done[1−7] even if the whole picture is still incomplete. In fact, there are some systems in which the thermodynamic properties of the intermetallic compounds, as expected from phase diagrams, are completely or partially lacking or sometimes scattered.

The scope of this work is to study the thermodynamics of the Ni-rich intermetallic compound, $Me_2Ni_{17}$, in three very similar Me-Ni systems with Me equal to Sm, Dy, and Yb. No thermodynamic data are reported in the literature for them and lanthanide intermetallic data can contribute to the assesment of the thermodynamic behavior in related systems. The high vacuum experimental setup adopted in the present work is based on a solid-state electrochemical cell inserted in a Knudsen-type holder. This setup makes it possible to overcome several problems well-known in the practice of the solid-state electrochemistry at atmospheric pressure of inert gases when using very reactive and volatile electrode materials. As far as the authors know, the above technique was never used before at least for the present purposes. The following section supplies the necessary information for a correct understanding of the whole paper.

## 2. Emf Measurements under Effusion Conditions

To improve the experimental setup already reported in the literature[8] and increase the reliability of emf measurements in the case of the determination of thermodynamic properties of rare earths intermetallics, we inserted the $CaF_2$ electrolyte galvanic cell in a tight space similar to a Knudsen's cell. This becomes mandatory when the vapor pressure of one of the components of the intermetallic compound is high at the operating temperatures of the electrochemical cell. In this way, and under high vacuum, the vaporization equilibrium is reached in a relatively short time and the reproducibility of emf data becomes significantly better.

Consider the electrochemical cell with $CaF_2$ single crystal (s.c.) as solid electrolyte in the general form:

$$(-)\mathrm{Pt/Me, Me}_x\mathrm{F}_y/\mathrm{CaF}_2\text{s.c./Me}_h\mathrm{Me}'_k, \mathrm{Me}_l\mathrm{Me}'_m, \mathrm{Me}_x\mathrm{F}_y/\mathrm{Pt}(+) \quad (1)$$

* Corresponding author. E-mail: Daniele.Gozzi@uniroma1.it.

10.1021/jp0142785 CCC: $22.00 
Published on Web 03/28/2002

where the overall cell reaction, 2e, is given by

$$x\mathrm{Me(s)} + y\mathrm{F}^- = \mathrm{Me}_x\mathrm{F}_y\mathrm{(s)} + y\mathrm{e} \quad (2a)$$

$$q\mathrm{Me(s)} = q\mathrm{Me(g)} \quad (2b)$$

$$(x+q)\mathrm{Me(s)} + y\mathrm{F}^- = q\mathrm{Me(g)} + \mathrm{Me}_x\mathrm{F}_y\mathrm{(s)} + y\mathrm{e} \mid \beta \quad (2c)$$

$$\alpha\mathrm{Me}_h\mathrm{Me}'_k\mathrm{(s)} + \beta\mathrm{Me}_x\mathrm{F}_y\mathrm{(s)} + \beta y\mathrm{e} = \gamma\mathrm{Me}_l\mathrm{Me}'_m\mathrm{(s)} + \beta y\mathrm{F}^- \mid 1 \quad (2d)$$

$$\beta(x+q)\mathrm{Me(s)} + \alpha\mathrm{Me}_h\mathrm{Me}'_k\mathrm{(s)} = \gamma\mathrm{Me}_l\mathrm{Me}'_m\mathrm{(s)} + q\beta\mathrm{Me(g)} \quad (2e)$$

in which semicell reactions 2c and 2d occur, respectively, at negative and positive electrodes.

The solid-state reaction forming the intermetallic $\mathrm{Me}_l\mathrm{Me}'_m$(s) is obtained as

$$\beta(x+q)\mathrm{Me(s)} + \alpha\mathrm{Me}_h\mathrm{Me}'_k\mathrm{(s)} = \gamma\mathrm{Me}_l\mathrm{Me}'_m\mathrm{(s)} + q\beta\mathrm{Me(g)} \quad (2e)$$

$$q\beta\mathrm{Me(g)} = q\beta\mathrm{Me(s)} \quad (2f)$$

$$x\beta\mathrm{Me(s)} + \alpha\mathrm{Me}_h\mathrm{Me}'_k\mathrm{(s)} = \gamma\mathrm{Me}_l\mathrm{Me}'_m\mathrm{(s)} \quad (2g)$$

The free energy change of reaction 2g, $\Delta_r G$, is given by

$$\Delta_r G = \Delta G_{\mathrm{cell}} - q\beta\Delta_v G \quad (3)$$

where $\Delta G_{\mathrm{cell}}$ and $\Delta_v G$, the free energy change of vaporization, are related to reactions 2e and 2f, respectively. $\Delta G_{\mathrm{cell}}$ is directly measured by the emf, $E$, of the cell through the well-known equation

$$\Delta G_{\mathrm{cell}} = -\beta y F E \quad (4)$$

$q$ is a number the meaning of which will be discussed later on.

From eq 3 and taking into account reactions 2e and 2g and also by comparison of the equations below,

$$\begin{cases} \Delta_r G = \Delta G^\theta_{\mathrm{cell}} + \beta RT \ln[a^q_{\mathrm{Me}}(g)/a^{x+q}_{\mathrm{Me}}] - q\beta\Delta_v G^\theta - q\beta RT \ln[a_{\mathrm{Me}}(g)/a_{\mathrm{Me}}] \\ \quad = \Delta G^\theta_{\mathrm{cell}} - q\beta\Delta_v G^\theta - x\beta RT \ln a_{\mathrm{Me}} \quad (2e) \\ \Delta_r G = \Delta_r G^\theta - x\beta RT \ln a_{\mathrm{Me}} \quad (2g) \end{cases} \quad (5)$$

one obtains that

$$\Delta_r G^\theta = \Delta G^\theta_{\mathrm{cell}} - q\beta\Delta_v G^\theta = x\beta RT \ln a_{\mathrm{Me}}(\mathrm{eq}) \quad (6)$$

In the above equations, $a_{\mathrm{Me}}$ is the activity of Me in the negative electrode and $a_{\mathrm{Me}}$(eq) is the activity of Me at the thermodynamic equilibrium between the two intermetallic phases $\mathrm{Me}_h\mathrm{Me}'_k$/$\mathrm{Me}_l\mathrm{Me}'_m$ in the positive electrode. $a_{\mathrm{Me}}(g)$ is the activity of Me in the gaseous phase. If $a_{\mathrm{Me}} = 1$ in the negative electrode, as in the present work, it follows that

$$\Delta_r G = \Delta_r G^\theta = \Delta G^\theta_{\mathrm{cell}} - q\beta\Delta_v G^\theta \quad (7)$$

From eqs 4 and 7, the measured standard emf, $E^\theta$, of the cell can be written as

$$E^\theta = -\frac{1}{y\beta F}(\Delta_r H^\theta + q\beta\Delta_v H^\theta) + \frac{T}{y\beta F}(\Delta_r S^\theta + q\beta\Delta_v S^\theta) \quad (8)$$

Through eq 8, the thermodynamic quantities

$$\Delta_r H^\theta_{\bar{T}} = -y\beta F\iota - q\beta\Delta_v H^\theta_{\bar{T}} \quad (9)$$

$$\Delta_r S^\theta_{\bar{T}} = y\beta F\sigma - q\beta\Delta_v S^\theta_{\bar{T}} \quad (10)$$

can be obtained by the intercept, $\iota$, and slope, $\sigma$, of the straight-line $E^\theta$ vs $T$ provided the thermodynamic data of Me vaporization are known as function of temperature. $\bar{T}$ is the average temperature in the experimental temperature range.

In isothermal and steady-state conditions, the net effusion flow-rate, $J_{\mathrm{Me,net}}$, is given by the Hertz−Knudsen's equation:[9]

$$J_{\mathrm{Me,net}}\ (\mathrm{mol/m^2\ s}) = \alpha_v P_e[1 - (P/P_e]/(2\pi M_{\mathrm{Me}}RT)^{1/2} = \alpha_v J_{\mathrm{Me},e}[1 - (P/P_e)] \quad (11)$$

where $M_{\mathrm{Me}}$ is the atomic mass of Me and $\alpha_v$ the vaporization coefficient, which is ≈1 for metals. $P_e$ and $P$ are the saturated vapor pressures of Me, respectively, at equilibrium and out of equilibrium. $J_{\mathrm{Me},e}$ is the mass flow-rate at the thermodynamic equilibrium given by the Knudsen's equation $J_{\mathrm{Me},e}\ (\mathrm{mol/m^2\ s}) = P_e/(2\pi M_{\mathrm{Me}}RT)^{1/2}$. The quantity $q$ is given by the ratio $J_{\mathrm{Me,net}}/J_{\mathrm{Me},e}$. Through eq 11, eq 7 becomes

$$\Delta_r G = \Delta_r G^\theta = \Delta G^\theta_{\mathrm{cell}} - \beta\alpha_v[1 - (P/P_e)]\Delta_v G^\theta \quad (12)$$

Therefore, the $\Delta_r G^\theta$ value depends also on the ratio $P/P_e$. When $P/P_e = 1$ ($q = 0$), no net mass and energy transfer occur from the electrochemical cell to the environment because $\Delta_v G_{\mathrm{Me}} = RT \ln(P/P_e) = 0$. This implies $\Delta_r G^\theta = \Delta G^\theta_{\mathrm{cell}}$. In the other cases, the electrochemical cell behaves as an open system in which the energy required to vaporize Me is supplied by the electrochemical cell itself ($P/P_e \ll 1$, $q \approx 1$) or, when oversaturation conditions are encountered ($P/P_e \gg 1$, $q < 0$), the energy is released to the cell from the gas phase through a net flow-rate of condensation. An energy flow-rate, $J_E = J_{\mathrm{Me,net}}\Delta_v G_{\mathrm{Me}}$ is associated to the net mass flow-rate $J_{\mathrm{Me,net}}$.

The change of emf with time, $\Gamma$, can be calculated by differentiating eq 12 with respect to the time and then equating it to zero since $(\partial\Delta_r G^\theta/\partial t)_T = 0$:

$$\Gamma = \left(\frac{\partial E^\theta}{\partial t}\right)_T = -\frac{\alpha_v RT}{yF}\frac{\ln(P_e/P^\theta)}{P_e}\left(\frac{\partial P}{\partial t}\right)_T = -\frac{\alpha_v RT}{yF}\frac{\ln(P_e/P^\theta)}{P_e}\left(\frac{\partial \ln P_t}{\partial t}\right)_T \quad (13)$$

$P_t$ is the total pressure inside the furnace that is continuously measured in the whole experiment. In deriving eq 13, the relation $dP_t = P_t\, dP$ has been used.

In the present work, the following points should be considered:

i. Me is the rare earth element, and Me′ = Ni.

ii. $\mathrm{Me}_l\mathrm{Me}'_m$ is the Ni-rich intermetallic compound in the Me-Ni phase diagram with $l = 2$ and $m = 17$. $\mathrm{Me}_h\mathrm{Me}'_k$ is the solid solution, $\mathrm{Ni_{ss}}$, produced by the eutectic reaction $\mathrm{L} \leftrightarrow \mathrm{Me_2Ni_{17}(s)} + \mathrm{Ni_{ss}}$ where $k = 1 - h$ and $0 < h \leq 5 \times 10^{-3}$ being $h$ the solid solubility of the rare earth element in Ni.

iii. The coefficients $h$, $k$, $l$, and $m$ are known and linked among them through the stoichiometric equations

$$\alpha h + \beta x = \gamma l$$

$$\alpha k = \gamma m$$

**TABLE 1: Vaporization Quantities of Metals Involved in the Present Work**

| Me | $M_{Me}$/g mol$^{-1}$ | $P_e$/mbar[a] at 1000 K | $J_{Me,e}$/mol m$^{-2}$ s$^{-1}$ | $P/P_e$[b] at 1000 K | $J_{Me,net}$/mol m$^{-2}$ s$^{-1}$ | $\Delta_v G_{1000}$/kJ mol$^{-1}$ | $J_E$/kW m$^{-2}$ |
|---|---|---|---|---|---|---|---|
| Sm | 150.36 | $1.1 \times 10^{-2}$ | $1.3 \times 10^{-2}$ | $9 \times 10^{-5}$ | $1.3 \times 10^{-2}$ | −78 | −1 |
| Dy | 162.50 | $1.6 \times 10^{-6}$ | $1.7 \times 10^{-8}$ | ≈1 | ≈0 | ≈0 | ≈0 |
| Yb | 173.06 | 5.4 | 5.7 | $2 \times 10^{-7}$ | 5.7 | −129 | −735 |
| Ni | 58.69 | $2.1 \times 10^{-12}$ | $1.3 \times 10^{-13}$ | $5 \times 10^{5}$ | | 109 | |

[a] Reference 13. [b] Calculated assuming $P \approx P_t = 1 \times 10^{-6}$ mbar.

Since $x = 1$ in $Me_xF_y$ and one mole of $Me_lMe'_m(s)$ is formed in reaction 2g, i.e., $\gamma = 1$, $\alpha = m/k = 17/(1 - h)$, and $\beta = l - (hm/k) = (2 - 19h)/(1 - h)$.

iv. Due to the trivalent state of Me in the respective fluorides, $y = 3$.

Some vaporization data, calculated at 1000 K according to eq 11, are reported in Table 1 where the calculations have been carried out by assuming $\alpha_v = 1$ and $P \approx P_t = 1 \times 10^{-6}$ mbar.

In practice, since the time interval, $\Delta t$, of an isotherm is in the order of a few hours, the emf values used to obtain the $E^\theta$ vs $T$ plot according to eq 8 were each one the average of the emf values over $\Delta t$ of each isotherm. This produces a negligible error with respect to the overall error associated to the thermodynamic data obtained (see the Discussion section).

Therefore, reaction 2g becomes

$$[(2-19h)/(1-h)]\mathrm{Me(s)} + [17/(1-h)]\mathrm{Me}_h\mathrm{Ni}_{1-h}(s) = \mathrm{Me}_2\mathrm{Ni}_{17}(s) \quad (14)$$

In principle, to obtain the reaction of formation of $Me_2Ni_{17}$, reaction 14 should be combined with reaction

$$[17h/(1-h)]\mathrm{Me(s)} + 17\mathrm{Ni(s)} = [17/(1-h)]\mathrm{Me}_h\mathrm{Ni}_{1-h}(s) \quad (15)$$

which is the formation reaction of the solid solution $Me_hNi_{1-h}$. Due to the negligible value of $h$, reaction 14 can be reasonably considered as the reaction of $Me_2Ni_{17}(s)$ formation. For this reason, in the thermodynamic data which follow, the subscripts "r" and "f" will be indifferently used.

It is important to point out that $\Delta G_{cell}$ (reaction 2e), i.e., the emf of the cell depends also on the activity of Me in the gaseous phase, whereas $\Delta_r G$ (reaction 2g) is independent of it. This requires that the thermodynamic reversibility should be ensured not only in the electrochemical cell but also between the electrochemical cell and the gaseous phase. The requisite criteria are achieved by confining the electrochemical cell in a tight place.

## 3. Experimental Section

**Cell Assembly.** The emf measurements were carried out in a high-vacuum horizontal furnace using a stainless steel, SS, spring-loaded latticework (see Figure 1) for positioning the holder of the electrochemical cell in the isothermal zone of the furnace. The holder is machined from a workable alumina rod (Aremco, USA) containing the electrodes, electrolyte, and Mo lead wires. Two small holes (1 mm diameter) serve as an outlet for the Mo wires and cell outgassing. All the components of the cell were shaped as small cylinders assembled as a sandwich in which the electrolyte is in the middle. The electrolyte is a polished disk of $CaF_2$ monocrystal (Crismatec, France) (111) oriented, 2 mm thick, and 8 mm in diameter. The electrodes have been prepared according to the criterion of establishing the polyphasic coexistence through a quite close contact between the powder particles. Following the well-established standard procedure, the pure solid phases, as fine powders, have been

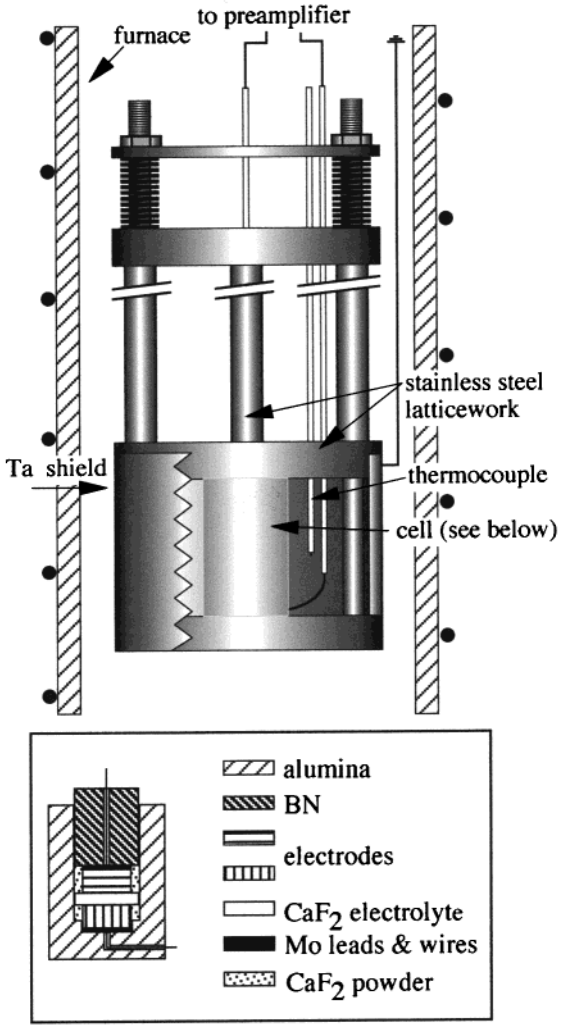


**Figure 1.** The experimental setup.

mixed in acetone and, after evaporation of the solvent, pressed in a stainless steel mold for obtaining cylinders 6 mm diameter × 3−5 mm height. All the pure rare earths metals (99.9%, 40 mesh) and their respective fluorides (99.99%, 325 mesh), both as powders, were purchased from Aldrich. The flat surfaces of electrodes were gently polished in such a way as to be in perfect contact with the electrolyte surfaces. The total length of the cells was never greater than 12 mm. The electrical leads were realized by Mo wires up to the feedthrough of the furnace flange. The temperature was measured by two S-type (Pt/Pt−Rh 10%) thermocouples positioned close together and with their longitudinal axis parallel and coplanar with the longitudinal axis of the cell. The distance between the axes was 10 mm and the spot-welded tips of the thermocouples have been placed in the plane orthogonal to the longitudinal axis of the cell and passing in the middle of the electrolyte disk. The temperature difference between the center of the electrolyte disk and the point where the thermocouples were positioned was measured to be −14 K

in the entire temperature range explored. The average value of the temperatures read by the two thermocouples was corrected accordingly. No detectable temperature difference was found between the electrode leads so there is confidence that the values of the cell emf do not need correction for superimposed thermoelectrical emfs. To have a uniform temperature around the cell a cylindrical cap-shaped Ta shield was positioned in the high temperature side of the latticework (see Figure 1). This shield combines two additional functions: to work as getter of the oxygen and moisture traces, and as a grounded shield to avoid possible noise on the emf signal induced by AC pickup from the furnace power supply. Before starting the emf measurements, the system was carefully flushed with Ar ($O_2$ < 1 ppm, $H_2O$ < 1 ppm) and then outgassed by following a standard procedure which does not allow an increase in the temperature of the cell if the pressure inside the furnace is greater than $5 \times 10^{-6}$ mbar. This procedure requires at least 12 days. The total pressure during the experiment is maintained at $1 \times 10^{-6}$ mbar. This lengthy procedure is necessary to reduce the content of oxidizing species at levels lower than the levels achievable by using purified Argon at atmospheric pressure instead of high vacuum. The emf measurements effected by means of a high impedance preamplifier ($10^{15}$ ohm, typical bias current 40 fA) connected to one of the analogue input channels of a data logger. The total accuracy in reading the emf recorded was less than 50 $\mu$V. Furnace temperature and pressure as well as the emf were read by the data logger connected to a personal computer. The measurements are real time monitored by a homemade software developed on the LabVIEW platform. The stability of the temperature of the furnace at the set temperature was always within 2 K. The temperature changes throughout the experiments were performed by programmed ramps with a slope of |0.3| K/min.

**Synthesis of $Me_2Ni_{17}$ Intermetallics.** Samples are alloys 91−94 at. % Ni synthesized by melting components, rare earths 99.9 and Ni 99.99 wt % nominal purity. Samples were made by means of an induction furnace in alumina crucibles under argon, quenched from liquid form. Samples characterized by well-defined, equilibrated two-phase forms. To ensure homogeneity, each sample was remelted repeatedly. In several cases, the evaporation of small quantities of rare earth was observed. The microstructure of the alloys were studied using standard optical and electronic micrographic methods. Quantitative electron probe microanalysis was also carried out using an energy-dispersive X-ray analyzer (EPMA) to confirm the final composition of the samples. The X-ray analysis was carried out onpowder samples using the Debye method. The XRD spectra of the eutectic mixtures $Me_2Ni_{17} + Ni_{ss}$ are reported in Figure 2. Except for the most intense peak assigned to Ni (111) ($2\theta$ = 44.507°, JCPDS 04-0850), the other features are satisfactorily in agreement with the calculated spectra of the respective $Me_2Ni_{17}$ compounds.

The crystal structure of $Me_2Ni_{17}$ compounds is *hP*38 with prototype $Th_2Ni_{17}$. The lattice constants in pm are [847.1 (*a*), 804.9 (*c*)], [829.9 (*a*), 803.7 (*c*)], and [828.0 (*a*), 802.4 (*c*)], respectively, for $Sm_2Ni_{17}$, $Dy_2Ni_{17}$, and $Yb_2Ni_{17}$. Their composition is 89.47 at. % Ni.

The phase diagrams of the Me-Ni systems examined are given in Figure 3. Eight intermediate phases are reported in the Sm−Ni phase diagram as assessed by Su et al.:[10] SmNi and $SmNi_5$, which melt congruently at 1079 °C and 1430 °C, respectively and $Sm_3Ni$, $SmNi_2$, $SmNi_3$, $Sm_2Ni_7$, $Sm_5Ni_{19}$, and $Sm_2Ni_{17}$ which form by peritectic reaction. Three eutectic reactions were observed: L → $Sm_3Ni$ + SmNi (at 570 °C and 32 at. % Ni),

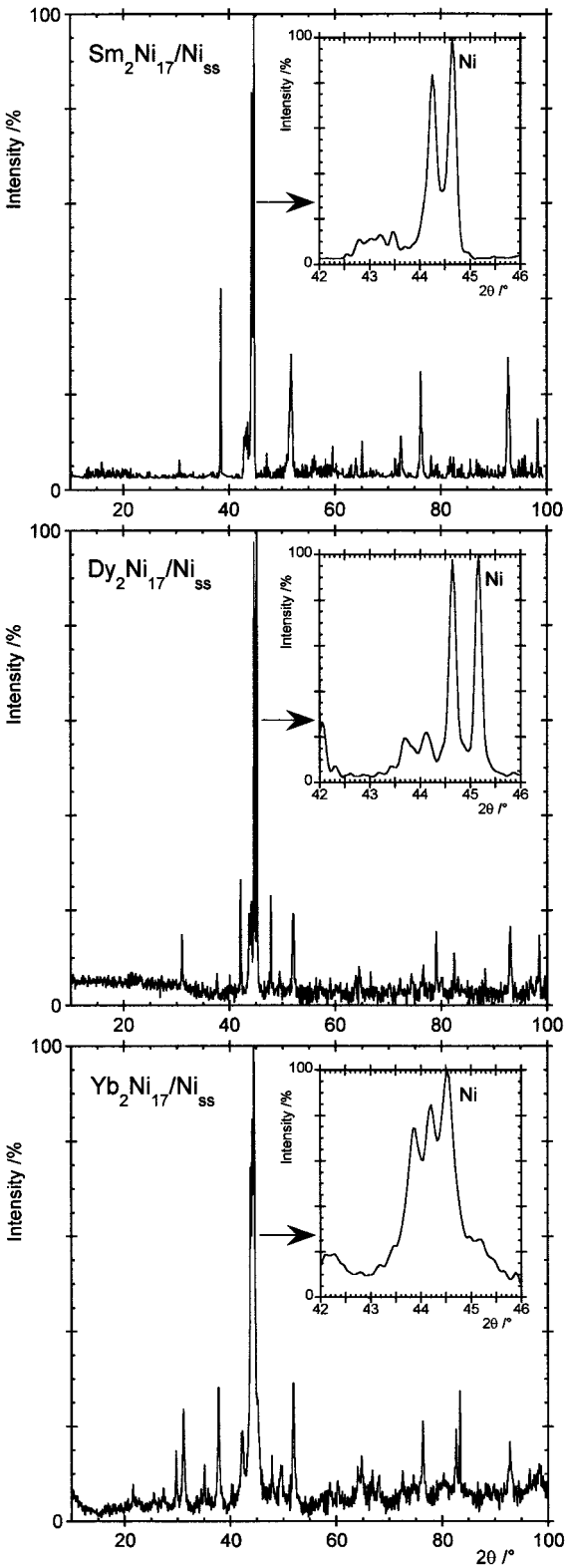


**Figure 2.** XRD normalized spectra of the synthesized $Me_2Ni_{17}/Ni_{ss}$ phases. X-ray source Cu K$\alpha_1$ ($\lambda$ =154.056 pm).

L → SmNi + $SmNi_2$ (at 809 °C and 53.5 at. % Ni) and L → $Sm_2Ni_{17}$ + $Ni_{ss}$ (at 1280 °C and 94 at. % Ni). However, in their work Su et al. pointed out that their description of the phase equilibria should be refined and more phase diagram experimental data are necessary.

The assessed Dy−Ni phase diagram is based primarily on the work of Cheng et al.,[11] who reported the existence of 10

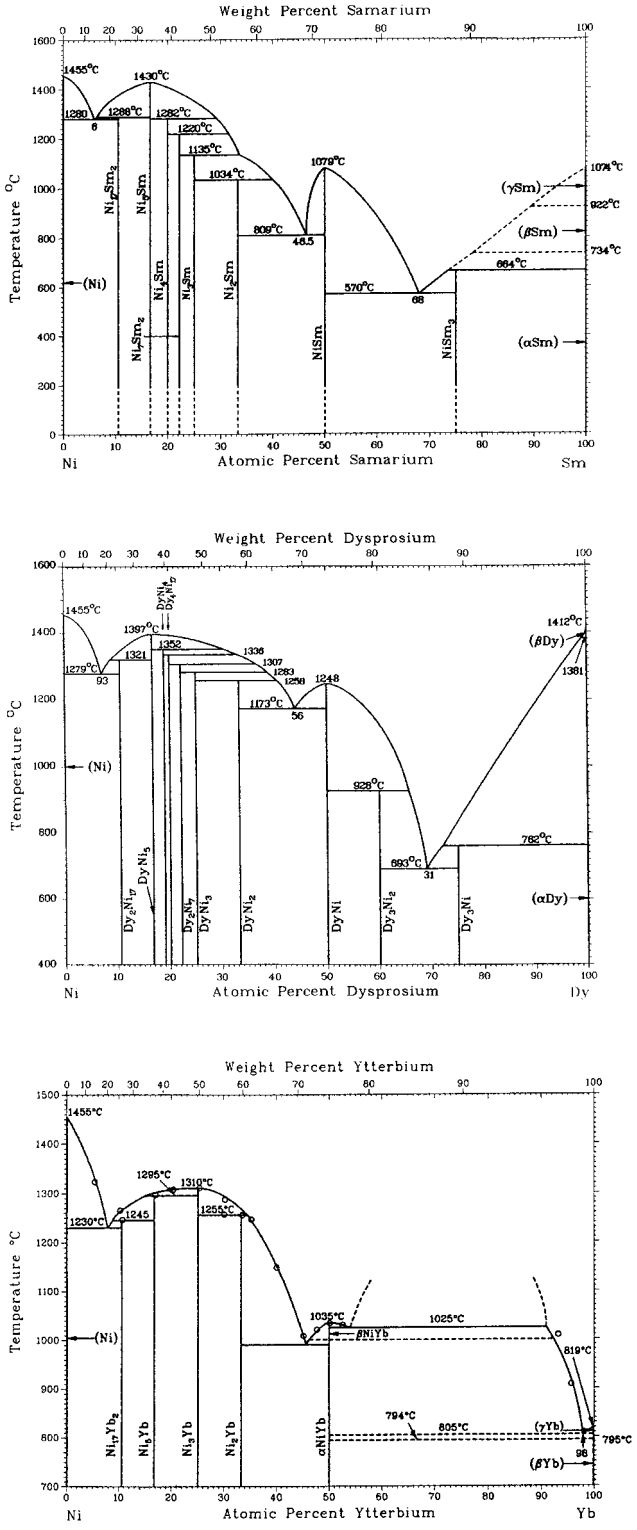


**Figure 3.** Phase diagrams of the examined Me-Ni systems. From top to bottom: Sm−Ni,[10] Dy−Ni,[11] and Yb−Ni.[12]

intermetallic compounds, and $Dy_3Ni$, $Dy_3Ni_2$, DyNi, $DyNi_2$, $DyNi_3$, $Dy_2Ni_7$, $DyNi_4$, $Dy_4Ni_{17}$, $DyNi_5$, and $Dy_2Ni_{17}$. DyNi and $DyNi_5$ melt congruently at 1248 and 1387 °C. $Dy_3Ni$, $Dy_3Ni_2$, $DyNi_2$, $DyNi_3$, $Dy_2Ni_7$, $DyNi_4$, $Dy_4Ni_{17}$, $DyNi_5$, and $Dy_2Ni_{17}$ form by peritectic reactions at 762, 928, 1258, 1283, 1307, 1336, 1352, and 1321 °C, respectively. Three eutectic reactions occur: L → $Dy_3Ni$ + $Dy_3Ni_2$ (at 693 °C and 31 at. % Ni), L → DyNi + $DyNi_2$ (at 1173 °C and 56 at. % Ni) and L → $Dy_2Ni_{17}$ + $Ni_{ss}$ (at 1279 °C and 93 at. % Ni).

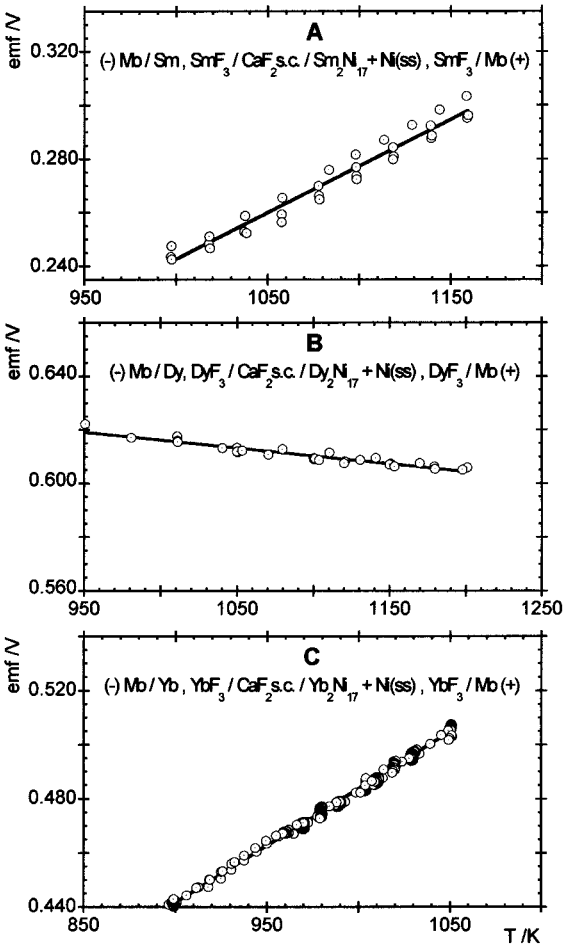


**Figure 4.** Experimental data of emf vs *T* obtained through $CaF_2$ electrolyte galvanic cells. The emf scale span is 100 mV. From A to C, the systems studied are $Sm_2Ni_{17}/Ni_{ss}$, $Dy_2Ni_{17}/Ni_{ss}$, and $Yb_2Ni_{17}/Ni_{ss}$.

The assessed Yb−Ni phase diagram is based primarily on the work of Palenzona et al.[12] The existence of five intermetallic phases has been established: YbNi, $YbNi_2$, $YbNi_3$, $YbNi_5$, and $Yb_2Ni_{17}$. As pointed out from several researchers, Yb behaves as trivalent in the Ni-rich alloy compositions. Very restricted terminal solid solubilities have been also established. A region of liquid immiscibility has been found for Yb-rich alloys, although its extent has not been determined other than at the monotectic temperature (1025 °C) where it extends from 54 to 91 at. % Yb.

## 4. Results

Figure 4 shows in parts A, B, and C the emf vs *T* plots for galvanic cells, such as to cell 1 in which Me is, respectively, Sm, Dy, and Yb. For comparison purposes, in all the above plots, the emf scale span has been set at 100 mV. Each plot consists of many experimental points, each point the result of an average of all the points read in the isotherm. The reading frequency was generally 1 point per minute and $\Delta t$ was within 1−3 h. The error bars on each point are calculated as the standard deviation on emf and *T*. The error bars are within the dimensions of the point. The thermal cycles were always programmed as stepwise cycles with increasing and decreasing ramps to avoid repeat at the same temperatures. The stepped cycle provides a check of the absence of hystereses, i.e., the reversibility of the emf behavior.

**TABLE 2: Thermodynamic Data of the Formation Reaction of $Me_2Ni_{17}$(s) Intermetallics**

| Me in $Me_2Ni_{17}$ | $\bar{T}$/K | no. of data points | $q$ | $\Delta_v H^\theta_{\bar{T}}$/ kJ mol$^{-1}$ [a] | $\Delta_v S^\theta_{\bar{T}}$/ J K$^{-1}$ mol$^{-1}$ [a] | $\Delta_f H^\theta_{\bar{T}}$ kJ/mol atom | $\Delta_f S^\theta_{\bar{T}}$/ J K$^{-1}$/mol atom | $\Delta_f \sim H^\theta_{298}$/ kJ/mol atom | $\Delta_f S^\theta_{298}$/ J K$^{-1}$/mol atom |
|---|---|---|---|---|---|---|---|---|---|
| Sm | 1084 | 32 | 1 | 207 ± 2 | 102.1 ± 0.3 | −17.9 ± 0.5 | −0.1 ± 0.3 | −14.6 ± 0.5 | |
| Dy | 1092 | 31 | 0 | 290 ± 4 | 110.2 ± 0.4 | −19.7 ± 0.1 | −1.72 ± 0.09 | −18.5 ± 0.1 | −2.05 ± 0.09 |
| Yb | 990 | 87 | 1 | 152.1 ± 0.8 | 102.5 ± 0.4 | −17.0 ± 0.1 | 1.96 ± 0.07 | | |

[a] Reference 13.

**TABLE 3: Calculation of $\delta_H$ and $\delta_S$**

| $Me_kNi_z$(s) | $T$/K | $T$/K | lit. ref | $(H^\theta_T - H^\theta_{T^\circ})^a$/ kJ/mol atom | $(H^\theta_T - H^\theta_{T^\circ})^b$/ kJ/mol atom | $\delta_H$ | $(S^\theta_T - S^\theta_{T^\circ})^a$/ J K$^{-1}$/mol atom | $(S^\theta_T - S^\theta_{T^\circ})^b$/ J K$^{-1}$/mol atom | $\delta_S$ |
|---|---|---|---|---|---|---|---|---|---|
| $SmNi_5$ | 1273 | 298 | 25 | 29.03 ± 0.22 | 33.3 ± 0.4 | 0.87 ± 0.02 | | | |
| $DyNi_5$ | 298.15 | 0 | 28 | 31 ± 2 | 32.8 ± 0.4 | 0.95 ± 0.07 | 11.93 | 11.8 ± 0.5 | 1.008 |
| $YbNi_5$ | | | | | | | | | |

[a] As given by the literature reference [b] As calculated through the Ivtanthermo tables[13] by using the Kopp rule.

The linear fit equations are

cell: (−)Mo/Sm, $SmF_3/CaF_2$s.c./$Sm_2Ni_{17}$ + Ni(ss), $SmF_3$/Mo(+)

$$\text{emf/V} = (-0.10 \pm 0.004) + (5.9 \pm 0.3) \times 10^{-4} T \quad (16)$$

cell: (−)Mo/Dy, $DyF_3/CaF_2$s.c./$Dy_2Ni_{17}$ + Ni(ss), $DyF_3$/Mo(+)

$$\text{emf/V} = (0.676 \pm 0.004) - (5.9 \pm 0.3) \times 10^{-5} T \quad (17)$$

cell: (−)Mo/Yb, $YbF_3/CaF_2$s.c./$Yb_2Ni_{17}$ + Ni(ss), $YbF_3$/Mo(+)

$$\text{emf/V} = (5.66 \pm 0.09) \times 10^{-2} + (4.213 \pm 0.009) \times 10^{-4} T \quad (18)$$

The calculated thermodynamic data obtained by applying eqs 9 and 10 to the eqs 16−18 are reported in Table 2. In the above calculation, $\beta = 1.915$ ($h = 5 \times 10^{-3}$) has been assumed. If $h$ were zero, i.e., $\beta = 2$ which means that $Me_2Ni_{17}$ is in equilibrium with pure Ni instead of $Ni_{ss}$, all the data in Table 2 of reaction 14 should be increased in absolute value by a quantity equal to 4.5%. No relevant modifications of the XRD spectra of electrodes were at the conclusion of the experiments.

## 5. Discussion

To compare and discuss the thermodynamic results reported in Table 2 with the literature data, it is necessary to use a reference temperature of 298.15 K. To do this, the heat capacities as function of temperature should be known for all the components of the reaction of formation of $Me_2Ni_{17}$ according to the well-known equations

$$\Delta_f H^\theta_{298} = \Delta_f H^\theta_{\bar{T}} + \sum_i \nu_i (H^\theta_{298} - H^\theta_{\bar{T}})_i \quad (19)$$

$$\Delta_f S^\theta_{298} = \Delta_f S^\theta_{\bar{T}} + \sum_i \nu_i (S_{298}{}^\theta - S^\theta_{\bar{T}})_i \quad (20)$$

where $\nu_i$ is the stoichiometric coefficient of the $i$th species in the formation reaction. Unfortunately, the enthalpy and entropy functions, respectively, $(H^\theta_T - H^\theta_{298})_{Me_2Ni_{17}}$ and $(S^\theta_T - S^\theta_{298})_{Me_2Ni_{17}}$ are lacking and should be estimated. Estimates are made by comparing the enthalpy function $(H^\theta_T - H^\theta_{298})$ of a given intermetallic $Me_wNi_z$ available in the literature with the same function calculated according to the Kopp (K) rule for the same intermetallic. In this way, the coefficient $\delta_H$ is found as

$$\delta_H = \frac{(H^\theta_T - H^\theta_{298})_{Me_wNi_z} \Leftarrow \text{from literature}}{(H^\theta_T - H^\theta_{298})_{Me_wNi_z} \Leftarrow \text{from K}} \quad (21)$$

In other terms, $\delta_H$ represents the deviation of the experimental value from the additivity rule of the heat capacities and its value is assumed to be the same also for another stoichiometry such as $Me_2Ni_{17}$, and at any other temperature $T \approx \bar{T}$. Therefore,

$$(H^\theta_T - H^\theta_{298})_{Me_2Ni_{17}} = \delta_H [(H^\theta_T - H^\theta_{298})_{Me_2Ni_{17}}]_K \quad (22)$$

and

$$\Delta_f H^\theta_{298} = \Delta_f H^\theta_{\bar{T}} + \{(H^\theta_{298} - H^\theta_{\bar{T}})_{Me_2Ni_{17}} - [2(H^\theta_{298} - H^\theta_{\bar{T}})_{Me} + 17(H^\theta_{298} - H^\theta_{\bar{T}})_{Ni}]\} = \Delta_f H^\theta_{\bar{T}} + (\delta_H - 1)[(H^\theta_{298} - H^\theta_{\bar{T}})_{Me_2Ni_{17}}]_K \quad (23)$$

being

$$[(H^\theta_{298} - H^\theta_{\bar{T}})_{Me_2Ni_{17}}]_K = [2(H^\theta_{298} - H^\theta_{\bar{T}})_{Me} + 17(H^\theta_{298} - H^\theta_{\bar{T}})_{Ni}] \quad (24)$$

The same procedure can be adopted for obtaining $\Delta_f S^\theta_{298}$ provided it is possible to calculate the deviation $\delta_S$ as ratio of entropy functions. The corrected values at 298 K are reported in Table 2. The values of $\delta_H$ and $\delta_S$ are given in Table 3 together data for their calculation. The empty cells in Table 3 mean that the data on any $Me_wNi_z$ intermetallic are unknown. The values of $[(H^\theta_{298} - H^\theta_{\bar{T}})_{Me_2Ni_{17}}]_K$ are −25.41, −24.64, and −21.40 kJ/mol atom for $Sm_2Ni_{17}$, $Dy_2Ni_{17}$, and $Yb_2Ni_{17}$, respectively. In the same order, the values of $[(S^\theta_{298} - S^\theta_{\bar{T}})_{Me_2Ni_{17}}]_K$ are −40.74, −39.54, and −36.48 J K$^{-1}$/mol atom. All the above values were calculated by using the Ivtanthermo tables.[13]

From the data reported in Table 2 and through eq 6, the $a_{Me}$(eq) values have been calculated by the equation below:

$$\log a_{Me}(\text{eq}) = (19/2.303\beta R)\,[(\Delta_f H^\theta_{298}/T) - \Delta_f S^\theta_{298}] \quad (25)$$

The respective log $a_{Me}$(eq) vs $1/T$ plots are shown in Figure 5. For comparison purposes, in plotting the curves of Figure 5, the uncorrected values of $\Delta_f H^\theta$ and $\Delta_f S^\theta$ have been utilized. At $T = 1000$ K, the activities are $6.8 \times 10^{-10}$, $4.8 \times 10^{-10}$, and $1.5 \times 10^{-10}$, respectively, for Sm, Dy, and Yb. In Table 4, the activities calculated at 1000 K for other $Me_2Ni_{17}/Ni_{ss}$ systems available in the literature are reported. Because both the phases $Me_2Ni_{17}$ and $Ni_{ss}$ are at thermodynamic equilibrium, the behavior of Me in the solid solution with Ni has also been considered. A tentative way to correlate the calculated activities through the atomic volume of Me is shown in Figure 6 where, with the

**TABLE 4: Comparison with the Literature Data**

| Me in $Me_2Ni_{17}$ | $Z$ | $T^a$/K | lit. ref | $\Delta_f H_T^\theta$/ kJ/mol atom | $\Delta_f S_T^\theta$/ J $K^{-1}$/mol atom | $-\log a_{Me}$(eq) at 1000 K | $-\Delta\bar{G}^{E}_{Me}$ [b]/ kJ/mol atom | $\Delta\bar{G}^{d}_{Me}$/ kJ/mol atom | $-\Delta\bar{G}^{e}_{Me}$/ kJ/mol atom |
|---|---|---|---|---|---|---|---|---|---|
| Y | 39 | 298 | 17 | −18.7 | | | | | |
| Sm | 62 | 1084[a] | this work | −17.8 ± 0.5 | −0.1 ± 0.3 | 9.17 | 132 | 150 | 282 |
| Gd | 64 | 873−1073 | 15 | −23.0 | −5.4 | 9.12 | 131[c] | 148[d] | 279[d] |
| Gd | 64 | 298 | 18 | −20.0 | | | | | |
| Dy | 66 | 1092[a] | this work | −19.7 ± 0.1 | −1.72 ± 0.09 | 9.32 | 134 | 134 | 268 |
| Er | 68 | 298 | 19 | −12.9 | | | | | |
| Yb | 70 | 990[a] | this work | −17.0 ± 0.1 | 1.96 ± 0.07 | 9.82 | 144 | 230 | 374 |
| Yb | 70 | 298 | 20 | −13.9 ± 1.0 | | | | | |
| Th | 90 | 973 | 21 | −24.8 | −1.8 | 11.9 | 184 | 147 | 331 |
| Pu(l) | 94 | 950−1080 | 22 | −9.0 | −1.5 | 3.89 | 30 | 30 | 60 |
| α-Pu | 94 | 950−1080 | 22 | −8.1 | 0.2 | 4.30 | 38 | 30 | 68 |
| Pu(l) | 94 | 913−1125 | 23 | −8.8 | −1.3 | 3.89 | 30 | 30 | 60 |
| α-Pu | 94 | 913−1125 | 23 | −7.8 | 0.4 | 4.25 | 37 | 30 | 67 |

[a] $T = \bar{T}$. [b] Calculated assuming 0.5% the solid solubility of Me in $Ni_{ss}$ and at 1000 K. [c] The value given in the related literature reference is −104 ± 5 kJ/mol atom. There, the Gd solid solubility in Ni and temperature were 0.10 ± 0.03 at. % and 1073 K, respectively. [d] The values of $\Delta\bar{G}^{d}_{Gd}$ and $\Delta\bar{G}^{e}_{Gd}$ in ref 15 are 149 ± 24 and −253 ± 29 kJ/mol atom, respectively.

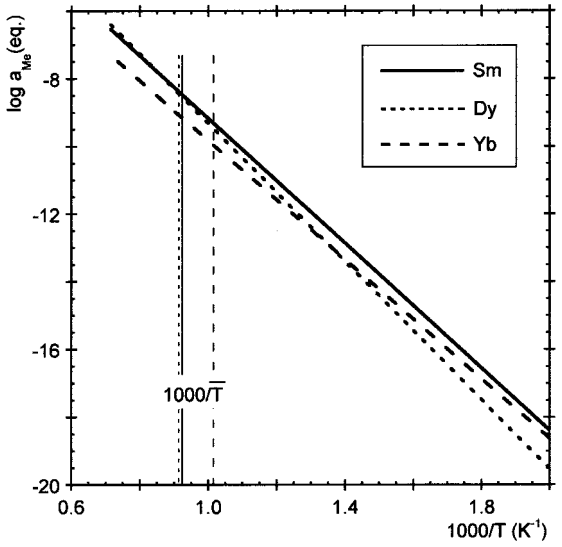


**Figure 5.** Activity of Me at equilibrium, $a_{Me}$(eq), between the phases $Me_2Ni_{17}$ and $Ni_{ss}$ as function of the reciprocal absolute temperature. The activity has been calculated according to eq 25.

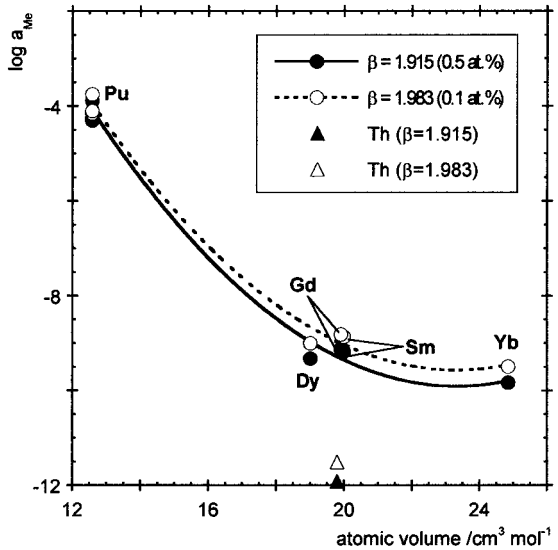


**Figure 6.** Activity of Me at equilibrium, $a_{Me}$(eq), against the atomic volume of Me. The curves have been calculated at solid solubilities 0.1 and 0.5 at. % of Me in Ni.

exception of Th, a regular trend appears. Two sets of data are reported in the above figure corresponding to two values of the solid solubility of Me in Ni: 0.1 and 0.5 at. %. The reported thermodynamic data of $Th_2Ni_{17}/Ni_{ss}$ could be affected by error especially looking at $\Delta_f H^\theta$ which is too negative in comparison with the other systems (see Table 4).

The values of the calculated activities imply that the thermodynamic behavior of the investigated rare earth elements in the solid solution with Ni is characterized by strong deviations from ideality. In fact, assuming the value of 0.5% the upper limit of Me solid solubility in Ni, we have to expect at 1000 K a value of the activity coefficient ranging from $3 \times 10^{-8}$ to $1 \times 10^{-7}$. The partial excess free energy of Me, $\Delta\bar{G}^{E}_{Me}$, has been calculated and reported in Table 4. Elsewhere,[14] as first approximation, $\Delta\bar{G}^{E}_{Me}$ has been considered as the sum of two excess terms $\Delta\bar{G}^{e}_{Me}$ and $\Delta\bar{G}^{d}_{Me}$. They are, respectively, associated to the electronic contribution due to the transfer of valence electrons from the Fermi level of Me to the Fermi level of Ni and the dilatation of Ni lattice upon the addition of Me. To reach the thermodynamic equilibrium, the electron transfer from Me to Ni occurs up to equalize the Fermi energies being $E_F(Me) > E_F(Ni)$. The lack of the values of the partial molar volume of Me, $\bar{V}_{Me}$, dissolved in Ni at infinite dilution does not allow the possibility to calculate separately the two contributions to $\Delta\bar{G}^{E}_{Me}$. An estimation can be attempted starting from both the literature data on $Gd_2Ni_{17}/Ni_{ss}$[15] and $\Delta\bar{G}^{d}_{Me}$:[14]

$$\Delta\bar{G}^{d}_{Me}(x_{Me}\rightarrow 0) = (B_{Ni}/b_{Ni})(\bar{V}_{Me} - V^0_{Ni}) + [(B_{Ni}/b_{Ni})V^0_{Ni}/(1 - b_{Ni})][1 - (\bar{V}_{Me}/V^0_{Ni})^{(1-b_{Ni})}] \quad (26)$$

where $V^0_{Ni}$, $B_{Ni}$, and $b_{Ni}$ are for Ni, respectively, the molar volume (6.59 $cm^3$/mol), bulk modulus at 1.013 bar ($1.92 \times 10^{11}$ $Nm^{-2}$),[16] and pressure coefficient of $B_{Ni}$, $(\partial B_{Ni}/\partial p)_T$ (7.969).[16] In fact, if one considers that $V^0_{Me}$ decreases almost regularly in the lanthanides with the exception of Ce, Eu, and Yb, a law of proportionality between $\bar{V}_{Me}$ and $V^0_{Me}$ in the $Me_2Ni_{17}/Ni_{ss}$ systems could be assumed. Since $\bar{V}_{Gd}$ is known (13.70 $cm^3$/mol) through the literature,[15] $\bar{V}_{Me} = (\bar{V}_{Gd}/V^0_{Gd})V^0_{Me}$, eq 26 can be computed and then both the contributions to $\Delta\bar{G}^{E}_{Me}$ can be found (see Table 4). The electronic contribution is always dominant with respect to the dilatational term due to the large difference between the Fermi levels, $E_F$, of Ni and lanthanides and Ni and actinides as well. The separate behaviors of $\Delta\bar{G}^{E}_{Me}$, $\Delta\bar{G}^{e}_{Me}$, and $\Delta\bar{G}^{d}_{Me}$ are shown in Figure 7 vs the difference of the Pauling electronegativity between Ni and Me, $\Delta_{Ni,Me}$. By

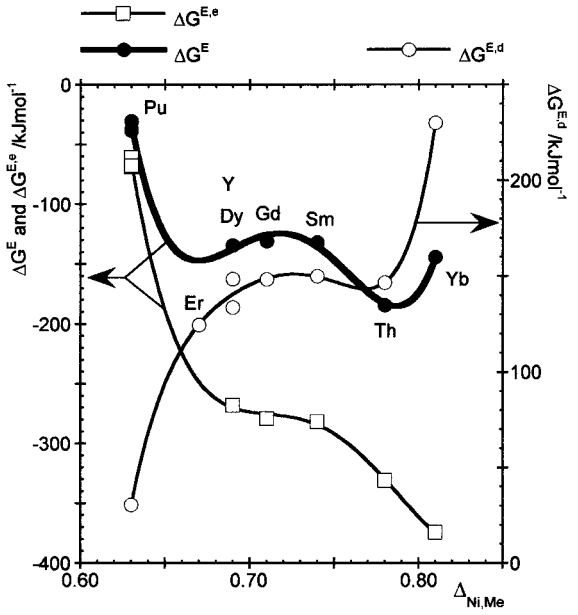


**Figure 7.** Partial excess free energy change, $\Delta\bar{G}^{E}_{Me}$ (left scale), against the electronegativity difference between Ni and Me. Both the components of $\Delta\bar{G}^{E}_{Me}$, electronic, $\Delta\bar{G}^{E,e}_{Me}$ (left scale), and dilatational, $\Delta\bar{G}^{E,d}_{Me}$ (right scale), are plotted.

inspection of Figure 7, it appears clear that small changes of $\Delta_{Ni,Me}$ can produce large changes in both the components of $\Delta\bar{G}^{E}_{Me}$ which have opposite trends. An increase of $\Delta_{Ni,Me}$ means that there is an increase in the ionic character which tends to strengthen the chemical bond. This implies also that Me with a larger electronic shell has therefore a larger atomic volume which requires more energy to expand the Ni lattice.

Table 4 compares also the thermodynamic data found in this work and thermodynamic data available in the literature[15,17−23] for the $Me_2Ni_{17}/Ni_{ss}$ system. With the exception of Pu data, the values of $\Delta_fH^\theta$ found in this work are comparable with a few values given in the literature even if a correct comparison is not feasible due to the lack of a common reference temperature. To check the consistency of the $\Delta_fH^\theta_{298}$ values experimentally determined in the Me-Ni field, the values found have been inserted in $\Delta_fH^\theta_{298}$ vs $x_{Me}$ plots together with all the available data[2,19,24−27] as drawn in the parts A to C of Figure 8. In part C, the value of $Yb_2Ni_{17}$ found in the present work is at 990 K. It is expected that the correction at 298 K gives a value very close both to the Miedema calculated and experimental value.[20] Though no experimental data are reported in the literature for $Sm_2Ni_{17}$ and $Dy_2Ni_{17}$, the values found in the present work strictly match the expected trends calculated by Miedema et al.[2] It is worth noting that most of the $\Delta_fH^\theta$ values listed in Table 4 could be affected by a small error due to formation of $Me_2Ni_{17}$, reaction 14, without taking into account reaction 15 which is the formation of the solid solution. In fact, very often data on the solid solubility are missing and when reported they are probably affected by large errors due to the intrinsic difficulty in measuring it. An indication of the solid solubility in Ni of the rare-earths elements can be obtained by examining the XRD spectra of Figure 2. It is easy to observe in the inserts of each diffraction pattern that the position of the most intense peak, corresponding to the (111) orientation of Ni, is shifted by a certain quantity depending on the rare earth element alloying with Ni. The shift, $\Delta d_{(111)}$, of the corresponding lattice parameter between the pure Ni and experimental ($Ni_{ss}$) value is expected to be a quantity linked to the solid solubility of Me

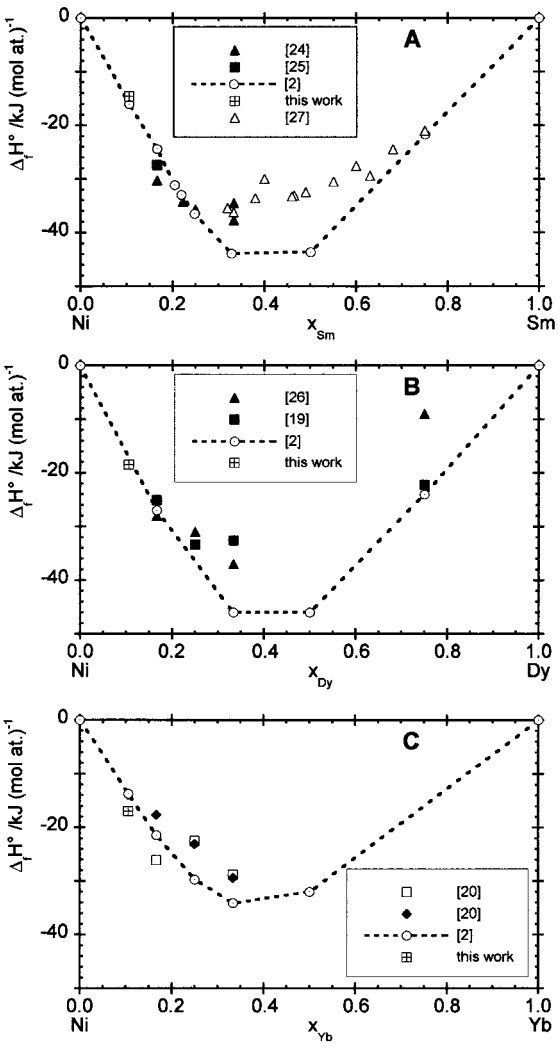


**Figure 8.** Standard enthalpy of formation at 298 K, $\Delta_fH^\theta_{298}$, of intermetallic phases in the Me-Ni systems examined. All the experimental and calculated data available in the literature are reported. The present results of $\Delta_fH^\theta_{298}$ of $Me_2Ni_{17}$ are compared. $\Delta_fH^\theta$ of $Yb_2Ni_{17}$ in part C is given at the average experimental temperature, 990 K.

in Ni which depends primarily on the atomic volume of Me. Increasing the difference, $\Delta V_{Me-Ni}$, between the atomic volume of Me and Ni, the Me solid solubility approaches both zero and $\Delta d_{(111)}$. This behavior is shown in Figure 9 where $\Delta d_{(111)}$ has been calculated by equation:

$$\Delta d_{(111)} = -\lambda\Delta\chi\cos(\chi/2)/4\sin^2(\chi/2) \qquad (27)$$

In the above equation, $\lambda$, $\chi$, and $\Delta\chi$ are, respectively, the Cu K$\alpha_1$ wavelength (154.056 pm), $2\theta$, and $\Delta(2\theta) = \chi[Ni_{(111)}] - \chi[Ni_{ss}]$. Therefore, among the systems studied, the solid solubility of Yb in Ni should be the lowest value, practically zero, i.e., $\beta \approx 2$. It is expected from eqs 9 and 10 that the related thermodynamic quantities of $Yb_2Ni_{17}$ (see Table 2), calculated with $\beta = 1.915$ (0.5 at. % of Yb in $Ni_{ss}$) should be increased accordingly by 4.4%, in absolute value ($\approx$0.7 kJ/mol atoms for $\Delta_fH^\theta_T$). By taking into account Figure 9, the values of $Sm_2Ni_{17}$ could be considered $\approx$3% more negative than the values given in Table 2.

An important point to consider, it is the comparison between the experimental and expected values of $\Gamma$ as calculated through eq 13. The typical isothermal trends of emf are reported in the

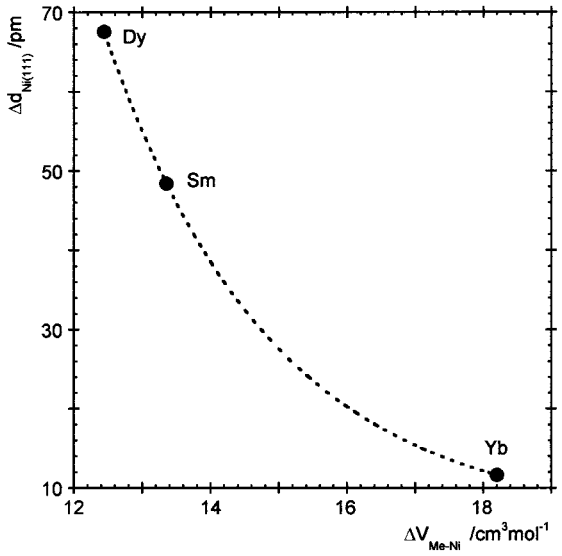


**Figure 9.** Change of lattice parameter of Ni as function of difference between the atomic volume of Me and Ni.

panels from Sm to Yb of Figure 10, respectively, for the three galvanic cells investigated. The Γ values, as slopes of the respective linear fits, are $\Gamma_{Sm}(1138) = -56 \pm 3$, $\Gamma_{Dy}(1120) = 0.3 \pm 1.2$, and $\Gamma_{Yb}(919) = -10 \pm 1$ nV s$^{-1}$. In the same order, the values of $(\partial \ln P_t/\partial t)_T$ are $-(3.3 \pm 0.3) \times 10^{-6}$, $-(1 \pm 1) \times 10^{-6}$, and $-(3.8 \pm 0.2) \times 10^{-6}$ s$^{-1}$. In parentheses are given the values of temperature in K. Notice that the value of $\Gamma_{Dy}$ in Figure 10 is much higher than the expected value which should be practically zero. This is because the emf vs *t* trend has been considered linear when it is actually a noise, and the reason that a large error is associated with it. The values of Γ calculated through eq 13 at the above temperatures are $\Gamma_{Sm}(1138) = -50$, $\Gamma_{Dy}(1120) = 1$, and $\Gamma_{Yb}(919) = -6$ nV s$^{-1}$. The comparison with the experimental values of Γ can be considered quite satisfactory. This is also evidence of reliability of the whole experiment and the thermodynamic data obtained.

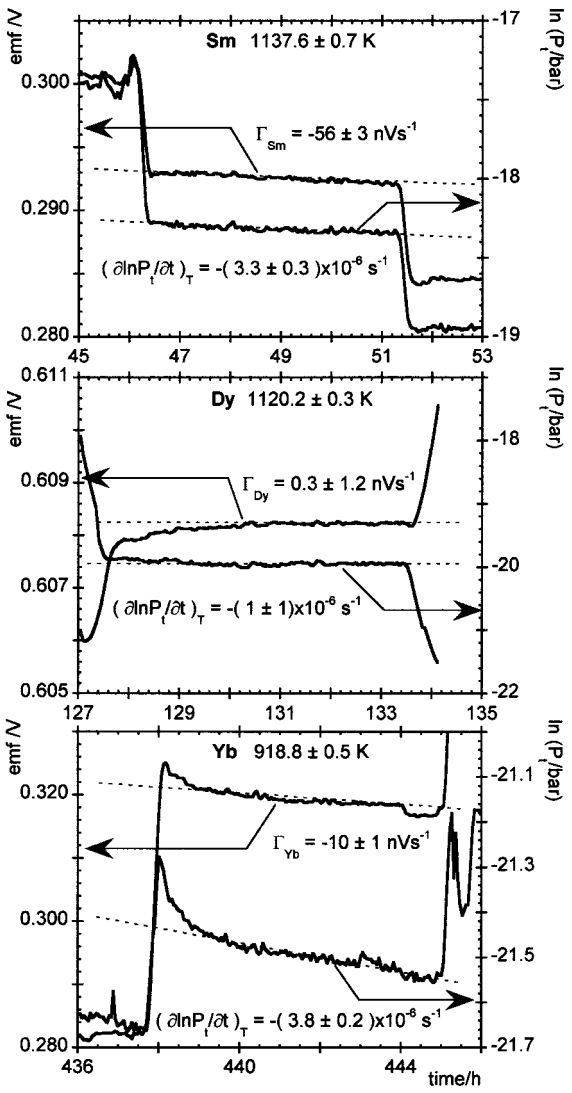


**Figure 10.** Typical experimental trends of emf (left scale) and total pressure (right scale) vs time at constant temperature.

## 6. Conclusions

The results are the experimental method and the thermodynamic data obtained through it. A primary use of emf measurements with respect to calorimetry is considered to complete the set of thermodynamic properties of the chemical system under study. For a variety of reasons, it is unfortunately not possible nor feasible to utilize all systems, because the reliability of the results is poor as a consequence of thermodynamic reversibility and/or electrochemical equilibrium which is not well-established. When the volatility of one or more components of the cell is high, the emf values vs temperature of solid-state galvanic cell, working in a conventional setup of inert gas environment at atmospheric pressure, is practically useless for deriving reliable thermodynamic data. The galvanic cell outlined in this paper makes it possible to overcome experimental difficulties without losing the required thermodynamic consistency. Besides the intrinsic source of error of the emf method which is often negligible, for example, in the present case if $q = 1$, an additional error is given only by the uncertainty on the vaporization data. Luckily, the uncertainty on $\Delta_v H^\theta$ and $\Delta_v S^\theta$ for metals is generally close to 1%. The general agreement that has been found between the present $\Delta_f H^\theta$ data of $Me_2Ni_{17}$, and the calculated or experimental trend along each Me-Ni system (see Figure 8) should be considered good evidence for the reliability of the experimental method. Most important, data found in this work on the $Me_2Ni_{17}$ intermetallics, until now unavailable in the literature, contribute to increase the knowledge of thermodynamics of the rare earth/3d transition metals systems.

**Acknowledgment.** The planning and development of the studies here presented form a part of an Italian National Research Project entitled "Leghe e Composti Intermetallici: stabilità termodinamica, proprietà fisiche e reattività". The authors thank the Ministero per la Ricerca Scientifica e Tecnologica (Programmi di rilevante interesse tecnologico) for the financial support. This work was also partially supported by CNR-Centro di Termodinamica Chimica alle Alte Temperature and Università di Roma "La Sapienza".

## References and Notes

(1) Brewer, L. *NATO ASI Ser., Ser. C* **1983**, *109*, 17.

(2) De Boer, F. R.; Boom, R.; Mattens W. C. M.; Miedema, A. R. *Cohesion in Metals, Transition Metal Alloys*; North-Holland: Amsterdam, 1988.

(3) Colinet, C.; Pasturel, A. *Handbook on the Physics and Chemistry of Rare Earths*; Gschneidner, K. A., Jr., Eyring, L., Eds.; North-Holland: Amsterdam, 1994; Vol. 19.

(4) Gschneidner, K. A., Jr. *J. Alloys Compd.* **1995**, *223*, 165.

(5) Colinet, C. *J. Alloys Compd.* **1995**, *225*, 409.
(6) Ferro, R.; Borzone, G.; Cacciamani, G.; Parodi, N. *Thermochim. Acta* **1998**, *314*, 183.
(7) Brewer, L. *Metall. Mater. Trans. B* **2000**, *31B*, 603.
(8) Borzone, G.; Ciccioli, A.; Cignini, P. L.; Ferrini, M.; Gozzi, D. *Intermetallics* **2000**, *8*, 203.
(9) Winterbottom, W. L. In *Physicochemical Measurements in Metals Research*; Rapp, R. A., Ed.; Interscience: New York, 1970; Vol. IV, Part I, Chapters 2A, 2B.
(10) Su, X.; Zhang, W.; Du, Z. *J. Alloys Compd.* **1998**, *278*, 182.
(11) Cheng, C. S.; Wang, C. *Acta Phys. Sin.* **1982**, *31*, 668.
(12) Palenzona, A.; Cirafici, S. *J. Less-Common Met.* **1973**, *33*, 361.
(13) *Ivtanthermo*; NIST special database 5; National Institute of Standards and Technology: Gaithersburg, MD, 1993.
(14) Schaller, H. J. *Ber. Bunsen-Ges. Phys. Chem.* **1983**, *87*, 734.
(15) Dischinger, J.; Schaller, H. J. *Ber. Bunsen-Ges. Phys. Chem.* **1998**, *102*, 1167.
(16) *Landolt-Börnstein, Tabellen und Funktionen*, 6th ed.; Springer: Berlin, 1971; Vol. 2, Part 1, p 425.
(17) Colinet, C.; Pasturel, A.; Buschow, K. H. J. *J. Appl. Phys.* **1987b**, *62*, 3712.
(18) Colinet, C.; Pasturel, A.; Buschow, K. H. J. *Metall. Trans. A* **1986**, *17*, 777.
(19) Schott, J.; Sommer, F. *J. Less-Common Met.* **1986**, *119*, 307.
(20) Brutti, S.; Ciccioli, A.; Balducci, G.; Gigli, G.; Borzone, G.; Raggio, R.; Ferro, R. *J. Phase Equilib.* **2002**, in press.
(21) Skelton, W. H.; Magnani, N. J.; Smith, J. F. *Metall. Trans.* **1970**, *1*, 1833.
(22) Campbell, G. M. *J. Chem. Thermodyn.* **1974**, *6*, 1110.
(23) Chiotti, P.; Akhachinskij, V. V.; Ansara, I.; Rand, M. H. In *The Chemical Thermodynamics of Actinide Elements and Compounds, Part 5: The Actinide Binary Alloys*; IAEA: Vienna, 1981.
(24) Pasturel, A.; Colinet, C.; Allibert, C.; Hicter, P.; Percheron-Guégan, A.; Achard, J. C. *Phys. Status Solidi B* **1984**, *125*, 101.
(25) Guo, Q.; Kleppa, O. J. *Metall. Mater. Trans.* **1998**, *29B*, 815.
(26) Buschow, K. H. J. *Permanent Magnet Materials Based on 3d-Rich Ternary Compounds*; Buschow, K. H. J., Wohlfarth, E. P., Eds.; 1990; Vol. 5 (Ferromagnetic Materials); Chapter 1.
(27) Borzone, G.; Parodi, N.; Raggio, R.; Ferro, R. *Alloys Comp.* **2001**, *317−318*, 532.
(28) Pan, Y. Y.; Nash, P. In *Phase Diagrams of Binary Nickel Alloys*; Nash, P., Ed.; ASM International: Materials Park, OH, 1991; p 99.